

Reinforcement Learning-based Non-Autoregressive Solver for Traveling Salesman Problems

Yubin Xiao, Di Wang, *Senior Member, IEEE*, Boyang Li, Huanhuan Chen, *Senior Member, IEEE*, Wei Pang, Xuan Wu, Hao Li, Dong Xu, Yanchun Liang, and You Zhou*

Abstract—The Traveling Salesman Problem (TSP) is a well-known combinatorial optimization problem with broad real-world applications. Recently, neural networks have gained popularity in this research area because they provide strong heuristic solutions to TSPs. Compared to autoregressive neural approaches, non-autoregressive (NAR) networks exploit the inference parallelism to elevate inference speed but suffer from comparatively low solution quality. In this paper, we propose a novel NAR model named NAR4TSP, which incorporates a specially designed architecture and an enhanced reinforcement learning strategy. To the best of our knowledge, NAR4TSP is the first TSP solver that successfully combines RL and NAR networks. The key lies in the incorporation of NAR network output decoding into the training process. NAR4TSP efficiently represents TSP encoded information as rewards and seamlessly integrates it into reinforcement learning strategies, while maintaining consistent TSP sequence constraints during both training and testing phases. Experimental results on both synthetic and real-world TSP instances demonstrate that NAR4TSP outperforms four state-of-the-art models in terms of solution quality, inference speed, and generalization to unseen scenarios.

Index Terms—Traveling Salesman Problem, graph neural network, reinforcement learning, non auto-regressive decoding.

I. INTRODUCTION

THE Traveling Salesman Problem (TSP) is one of the most well-known NP-hard problems [1] and can be defined on a connected graph with non-negative edge weights. A TSP solution is a Hamiltonian cycle that minimizes the sum of edge weights in the path. Here, the Hamiltonian cycle is a path that starts and ends at the same node and visits every other node exactly once. TSP has a wide range of real-world applications, such as maritime transportation [2], facility placement [3], and supply chain management [4]. Due to the NP-hard nature of

TSP, many approximate and heuristic algorithms [5], [6] have been developed over the years.

Recently, advances in deep learning have led researchers to develop neural networks (NNs) as a viable solver for TSPs [7]–[11]. While theoretical guarantees for such networks remain elusive, in practice, they tend to produce near-optimal solutions. However, most existing NN solutions adopt the autoregressive (AR) approach, which produces nodes on the Hamiltonian cycle one at a time. The sequential nature of these networks poses a fundamental limit on the speed of the algorithm. On the other hand, non-autoregressive (NAR) networks [12], [13] feature fast inference, but tend to produce comparatively low-quality solutions, especially when the test problems differ in size and distribution from those encountered during training [13].

This paper focuses on NAR networks for solving TSPs. We attribute the limited popularity of NAR models to the following three key limitations. First, conventional NAR models adopt supervised learning (SL) for training, requiring predetermined optimal solutions for numerous TSP instances as training data through exact TSP solvers (e.g., Concorde [14]), which is computationally expensive. Secondly, the SL-trained models are vulnerable to overfitting, leading to poor generalization performance on other TSPs. For instance, an unsatisfactory generalization ability is reported in [13]. Thirdly, their training process is not completely consistent with the inference process, resulting in less competitive performance. Specifically, they relax the sequential/tour constraint of TSP during training, estimating the importance of each edge in parallel. However, they impose such constraints in the inference phase, forming feasible TSP solutions by searching for essential edges.

To address the aforementioned limitations of conventional NAR models, we propose a novel NAR model called NAR4TSP with several improvements. First, we propose a modified architecture for the graph neural network (GNN), aiming to facilitate the discovery and optimization of Hamiltonian cycles by extracting information from graphs represented by TSPs. Specifically, we introduce a learnable pointer that indicates the starting node, whereas existing techniques [12], [13] always start at the first node. Our proposed GNN takes the node coordinates and distances between nodes as inputs, and outputs scores for all edges and the starting-node pointer. Secondly, to ensure the consistency of the sequential constraints of TSP being applied in both the training and inference phases, which is crucial for producing high-quality solutions in AR models [15]–[17], we impose the sequential constraints of TSP

(* Corresponding author: You Zhou)

Yubin Xiao, Xuan Wu, and You Zhou are with the Key Laboratory of Symbolic Computation and Knowledge Engineering of Ministry of Education, College of Computer Science and Technology, Jilin University, Changchun, 130012, China (e-mail: zyou@jlu.edu.cn).

Di Wang is with the Joint NTU-UBC Research Centre of Excellence in Active Living for the Elderly, Nanyang Technological University, 639798, Singapore.

Boyang Li is with the School of Computer Science and Engineering, Nanyang Technological University, 639798, Singapore.

Huanhuan Chen is with the School of Computer Science, University of Science & Technology of China, Hefei, 230026, China.

Wei Pang is with the School of Mathematical and Computer Sciences, Heriot-Watt University, Edinburgh EH14 4AS, U.K.

Hao Li is with College of Computer, National University of Defense Technology, Changsha, Hunan, 410073, China.

Dong Xu is with the Department of Electrical Engineering and Computer Science, Bond Life Sciences Center, University of Missouri, Columbia, USA.

Yanchun Liang is with the School of Computer Science, Zhuhai College of Science and Technology, Zhuhai 519000, China.

during training (i.e., not only during inference). Specifically, we decode the output of the GNN with such constraints to produce a TSP solution, which is then assessed and used as a reward for the self-critical reinforcement learning (RL) strategy [18]. Thirdly, we enhance the vanilla RL strategy for training our NAR models to perform better with fewer computing resources (see Section III-D for more details). Specifically, we leverage the one-shot nature of the NAR networks, replacing the two modules used in the vanilla RL strategy with a single module. Through RL training, NAR4TSP addresses the limitations of using SL in conventional NAR models, i.e., it does not require the expensively produced ground-truth labels.

It is worth noting that combining NAR network and RL technology appears challenging due to their contrasting nature. The NAR network produces parallel outputs, whereas the RL process demands a step-by-step implementation. However, we introduce a decoding process that progressively transforms the NAR network’s outputs into the TSP solutions, thus, seamlessly integrating RL into our approach. To the best of our knowledge, NAR4TSP is the first NAR model trained using RL for solving TSPs.

We evaluate NAR4TSP in three aspects, namely solution quality, inference latency, and generalization to unseen scenarios. We adopt ten neural network baselines [13], [15]–[17], [19]–[24] and compare them with NAR4TSP on TSP50 (TSP with 50 nodes) and TSP100 (TSP with 100 nodes). Despite the one-shot nature of NAR decoding [25], NAR4TSP produces competitive solutions while achieving significantly shorter inference time. To evaluate the inference speed of NAR4TSP, we measure its inference time and compare it to that of four state-of-the-art (SOTA) NN-based models [13], [15]–[17] using TSPs of different sizes and beam search with different widths. The experimental results show that NAR4TSP outperforms the other models in terms of inference speed, especially when the number of nodes and the width of beam increase. Finally, we evaluate the out-of-domain generalization of NAR4TSP to TSP instances of different sizes from that of training data and 25 real-world instances. The experimental results indicate that NAR4TSP has a superior generalization ability comparing against the other SOTA models [13], [15]–[17]. In addition to result comparisons, we demonstrate the feasibility of implementing NAR4TSP in an end-to-end manner and the effectiveness of NAR4TSP for solving TSPs through the visualization of the decoding process and the overall path planning of NAR4TSP, respectively.

The key contributions of this research work are as follows:

- To the best of our knowledge, we propose the first NAR model trained using RL for solving TSPs, eliminating the need for expensive ground-truth labels used to train the conventional SL-based NAR models.
- We construct a novel GNN as the backbone architecture of NAR4TSP and incorporate sequential constraints of TSP during training to elevate the model performance.
- We show the excellent performance of NAR4TSP, especially in inference speed and generalization ability, by conducting extensive experiments.
- We demonstrate NAR4TSP’s ease in implementation and effectiveness by visualizing its decoding process and

TABLE I
END-TO-END NN-BASED MODELS PROPOSED TO SOLVE TSPS

Decoding: Training:	AR	NAR
	SL	Vinyals <i>et al.</i> [19]
RL	Kool <i>et al.</i> [15]; Bresson and Laurent [16]; Jung <i>et al.</i> [17]; Bello <i>et al.</i> [20]; Khalil <i>et al.</i> [21]; Deudon <i>et al.</i> [22]; Wu <i>et al.</i> [23]; Ma <i>et al.</i> [26]; Nazari <i>et al.</i> [27]; Wang <i>et al.</i> [28]	NAR4TSP (our work)

overall path planning, respectively.

II. RELATED WORK

In this section, we review the conventional algorithms for solving TSPs and the relevant NN-based TSP solvers.

A. Conventional TSP Solvers

Conventional algorithms for solving TSPs can be generally classified into exact and approximate methods, as well as heuristics. The first category, exemplified by Concorde [14], is known to produce optimal TSP solutions through integer programming and optimization algorithms, including Cutting Planes and Branch-and-Bound [29]–[31]. The second category typically employs linear programming and relaxation techniques to produce TSP solutions with guaranteed quality [32]. The third category, represented by LKH3 [33] and its predecessor LKH2 [34], is based on the k -opt heuristics and has been shown to produce solutions almost as good as those generated by Concorde [35]. Additionally, evolutionary computation algorithms, such as ant colony optimization [36], [37] have been proposed to solve TSPs.

However, conventional TSP solvers may not be suitable for real-time TSP tasks due to their inability to produce high-quality solutions within a short time frame [38].

B. Neural Network-based TSP Solvers

With the recent advancements in deep learning, numerous NN-based models have been proposed to solve TSPs. These models can be generally categorized into AR or NAR according to their model decoding methods, and SL or RL according to their model training methods. It is worth noting that we focus on end-to-end learning methods for solving TSPs, and exclude neural improvement algorithms that combine deep learning and heuristic search because they typically have longer inference latency [35]. In Table I, we provide an overview of the difference between the existing end-to-end NN-based models and our work. In the remainder of this subsection, we first review the pioneering NN-based approaches used to solve TSPs, which adopt AR decoding and SL.

Vinyals *et al.* [19] proposed a sequence-to-sequence SL model named Pointer Network (PtrNet), which utilizes the Long Short-Term Memory (LSTM) architecture commonly used in natural language processing [39] for solving TSPs. PtrNet takes node coordinates as its input, employs the attention mechanism and generates TSP solutions step-by-step,

using the optimal solutions produced by Concorde as the ground-truth labels. While PtrNet provides a novel perspective for solving combinatorial optimization (CO) problems, its unsatisfactory performance and high cost of label production make it challenging to be applied in practical settings [38], [40]. Compared to SL models, which require optimal solutions at each step during training, RL is a more elegant alternative in the absence of ground-truth labels. Moreover, RL has demonstrated robust learning and optimized decision-making ability in AlphaGo Zero [41] and Atari [42]. Thus, majority existing AR approaches use RL for training, lifting the prerequisite of optimal solutions. For instance, Bello *et al.* [20] expanded PtrNet using the actor-critic RL algorithm, making it possible to train models without using the optimal solutions. Nazari *et al.* [27] further enhanced PtrNet’s performance by replacing the LSTM architecture of the encoder with an embedding of all nodes. With Transformer setting new performance records in various applications [43], numerous Transformer-based TSP models have been proposed, with the most promising ones being [15], [16], [22]. These three models adopt the same Transformer-encoder architecture but differ in the decoder architecture. Briefly speaking, when a decoder generates the probability distribution of nodes at time t , Deudon *et al.* [22] used the node information at time $t-1, t-2, t-3$ as the input; Kool *et al.* [15] used the node information at time $1, t-1$ as the input; and Bresson and Laurent [16] used the fusion of all previously output node information as the input, all of which demonstrated superior performance.

However, the type of step-by-step solution generation method used by AR models has a natural disadvantage in terms of inference speed when compared to the NAR approaches [44]. Additionally, due to the sequential nature of AR models, beam search suffers from diminishing returns with respect to the beam size and shows limited search parallelism [45]. To address these issues, several NAR models have been developed to improve the inference speed when solving TSPs [12], [13]. These models regard TSP as a link prediction problem that has been studied in various relevant research fields [46]–[48]. They use SL to train their models to estimate the importance of each edge belonging to the optimal solution. For instance, Nowak *et al.* [12] utilized a GNN-based TSP solver trained with SL. The model takes a TSP instance as a graph for model input and directly outputs a heat map that represents the importance of edges. It is worth noting that during training, the model relaxes the sequential constraint of TSP to obtain the edge’s importance by minimizing the binary cross-entropy loss between the adjacency matrix corresponding to the optimal solution and the heat map. While during inference, the model imposes such constraints by using greedy search or beam search on the heat map to obtain a feasible TSP solution. Subsequently, Joshi *et al.* [13] replaced the architecture of the aforementioned model [12] with a graph convolutional network (GCN), which achieved better performance.

Despite the significant improvement in inference speed offered by NAR approaches, the solution quality of these models is often suboptimal [12], [13]. In fact, existing NAR models generally fail to outperform most of the afore-reviewed AR models [25], [28]. As such, we deem there is a pressing

need to improve the existing models further to achieve high-quality solutions with low inference latency.

III. NAR4TSP

In this section, we present a novel NAR model named NAR4TSP, which is designed to better solve TSPs. As shown in Fig. 1, NAR4TSP adopts a unique GNN architecture to output a starting-node pointer and a matrix of edge scores. It then decodes the GNN’s output to produce feasible TSP solutions for model training. We detail the TSP setting, the architecture and decoding process of NAR4TSP, and the enhanced RL strategy of NAR4TSP in the following subsections, respectively.

A. TSP Setting

Our research focuses on the most fundamental Euclidean TSP due to its importance and prevalence in various domains [12], [13], [15], [16], [22]. We present a TSP instance as a graph $G = (V, E)$ with n nodes in the node set V , and $n \times n$ edges in the edge set E , where node $x_i^v \in \mathbb{R}^{n \times d}$ denotes the d -dimensional node coordinates and edge $x_{i,j}^e \in \mathbb{R}^{n \times n}$ denotes the Euclidean distance between nodes x_i^v and x_j^v .

We define a TSP tour as a permutation of n nodes denoted by $\pi = \{\pi_1, \pi_2, \dots, \pi_n\}$, where $\pi_i \neq \pi_j, \forall i \neq j$. The length of a TSP tour π is defined as follows:

$$L(\pi) = x_{\pi_n, \pi_1}^e + \sum_{i=1}^{n-1} x_{\pi_i, \pi_{i+1}}^e, \quad (1)$$

where x_{π_i, π_j}^e denotes the Euclidean distance between nodes π_i and π_j .

B. Architecture of NAR4TSP

As shown in Fig. 1, the architecture of NAR4TSP consists of three key components, namely 1) a linear layer for input embedding; 2) multiple GNN modules for facilitating information transfer among nodes, edges and the starting symbol, and ultimately for outputting the starting-node pointer; and 3) several fully-connected (FC) layers for outputting edge scores. For the ease of subsequent descriptions, we denote the number of GNN modules and FC layers as N_g and N_f , respectively.

It is worth noting that the TSP solution forms a Hamiltonian cycle, allowing any node to be selected as the starting node. Nevertheless, for guaranteeing the production of a valid solution, the implementation of a mask mechanism becomes necessary. This mechanism masks the probability of pointing to previously selected nodes, thereby preventing nodes from being revisited. Consequently, the resulting probability distribution of earlier node selections shows a more significant dispersion compared to the later selections, because the probability of selecting previously visited nodes at each selection is masked to zero. Therefore, the selection of the first node presents the most dispersed probability distribution, underscoring the challenge and significance of the selection of the starting node.

Drawing inspiration from natural language processing research, where special symbols (e.g., “*<bos>*”) serve various

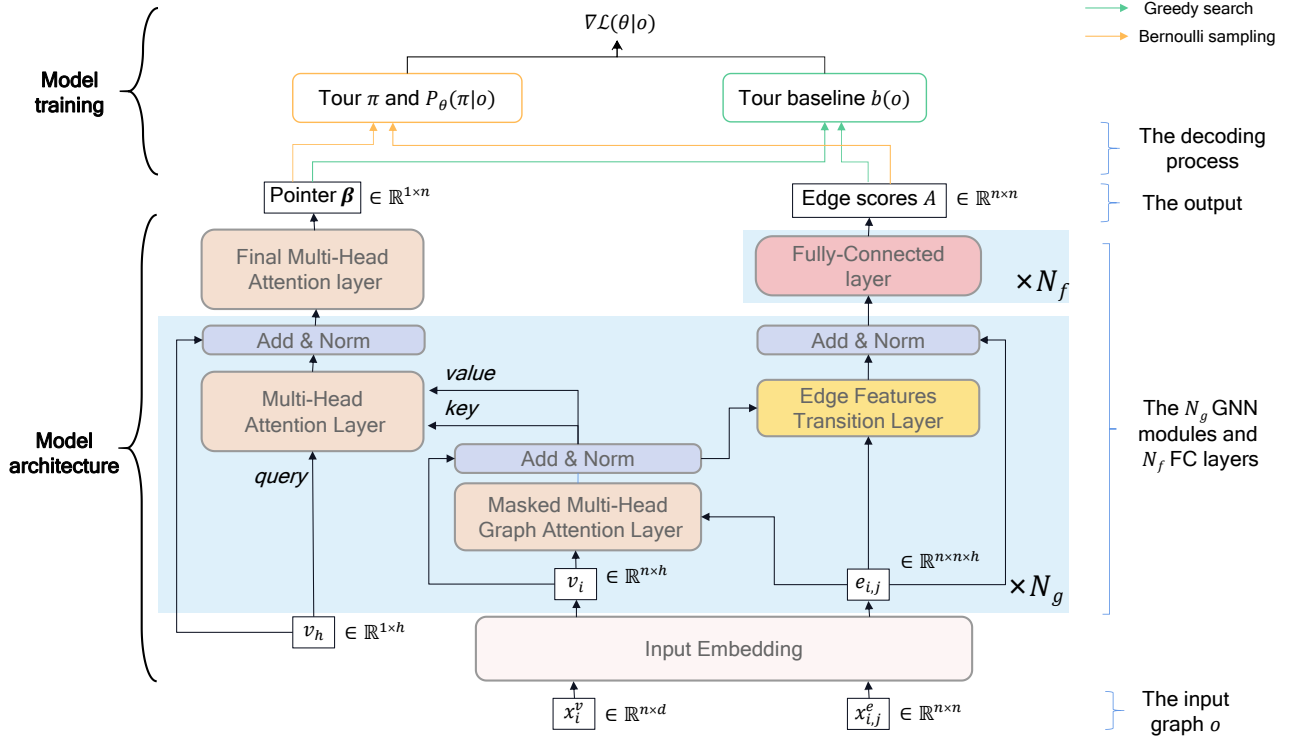


Fig. 1. The pipeline of NAR4TSP. Taking a TSP instance o with the node coordinate x_i^v and the Euclidean distance between nodes $x_{i,j}^e$ as inputs, the model starts by processing the information through a linear layer, transforming it into node features v_i and edge features $e_{i,j}$. The model then interacts with a randomly initialized learnable starting symbol v_h via N_g GNN modules, and finally outputs a starting-node pointer β and a matrix A of edge scores. The output β and A are subsequently decoded into a feasible TSP tour through sampling or greedy search. The solution is obtained in a one-shot, NAR manner, and its quality is treated as a reward and optimized by an enhanced RL strategy.

purposes, such as marking the beginning of a sentence [49]. We design the pointer in the GNN modules for the purpose of initiating the decoding at the most promising starting position to produce TSP solutions. This approach differs from conventional NAR models, which typically take the node indexed at 1 as the starting node [12], [13]. By utilizing the pointer mechanism, we establish a framework to incorporate the sequential constraint of TSP into the decoding process, thus applying the consistent sequential constraints in both training and inference phases, unlike the afore-reviewed NAR models [12], [13] (see Section II-B). To the best of our knowledge, this novel GNN architecture, featuring a starting-node pointer output, represents a pioneering architecture that leverages TSP representations to guide the decoding process in NAR models. The effectiveness of this novel architecture is assessed later through three ablation studies (see Section IV-D).

For a given TSP graph, NAR4TSP first linearly projects the input nodes $x_i^v \in \mathbb{R}^{n \times d}$ and edges $x_{i,j}^e \in \mathbb{R}^{n \times n}$ into h -dimensional features. Their initial embedding is as follows:

$$v_i^0 = \mathbf{W}_v x_i^v + \mathbf{b}_v, v_i^0 \in \mathbb{R}^{n \times h}, \quad (2)$$

$$e_{i,j}^0 = \mathbf{W}_e x_{i,j}^e + \mathbf{b}_e, e_{i,j}^0 \in \mathbb{R}^{n \times n \times h}, \quad (3)$$

where \mathbf{W} and \mathbf{b} denote the learnable parameters of weights and biases of the GNN, respectively.

NAR4TSP utilizes N_g GNN modules to extract feature information from the graph. GNN is a specific type of NN that is well-suited for information interaction between nodes and

edges in graphs, and its effectiveness has been demonstrated in prior studies [12], [13], [50]. In our work, each GNN module is used for three types of feature information transfer, namely nodes, edges, and the starting symbol. We detail these feature information transfer mechanisms in the subsequent paragraphs.

1) **Node:** For the transfer of node feature information, we integrate the edge features with the node features using the vanilla multi-head graph attention module [51]. Because it is trivial to extend single head to multi-head, we use a single head in all formulas for the convenience of subsequent descriptions, as done in [16]. As an initial step, we apply a linear transformation parameterized by a weight matrix to all nodes and edges, respectively. We then apply the LeakyReLU nonlinear activation function σ_1 and compute the importance of node j 's features to node i as follows:

$$\lambda_{i,j}^l = \sigma_1(\mathbf{W}_e^l \|\mathbf{W}_v^l [v_i^{l-1} \| v_j^{l-1}]\| \mathbf{W}_{ve}^l e_{i,j}^{l-1}), \lambda_{i,j}^l \in \mathbb{R}^{n \times n}, \quad (4)$$

$$\sigma_1(z) = \begin{cases} z, & \text{if } z > 0, \\ \delta z, & \text{otherwise,} \end{cases} \quad (5)$$

where $l \in \{1, 2, 3, \dots, N_g\}$ denotes the GNN module index, $\|$ denotes the concatenation operator, and δ denotes the trade-off parameter. To facilitate the comparison of importance scores across different nodes, we apply the Softmax activation function σ_2 to normalize them, which is defined as follows:

$$\alpha_{i,j}^l = \sigma_2(\lambda_{i,j}^l \odot N_{i,j}), \alpha_{i,j}^l \in \mathbb{R}^{n \times n}, \quad (6)$$

$$\sigma_2(z_i) = \frac{e^{z_i}}{\sum_{j=1}^n e^{z_j}}, \forall i \in \{1, 2, \dots, n\}, \quad (7)$$

$$N_{i,j} = \begin{cases} 1, & \text{if node } j \in N_{set(i)}, \\ -\infty, & \text{otherwise,} \end{cases} \quad (8)$$

where \odot denotes the element-wise multiplication and $N_{i,j}$ denotes the mask on whether node j belongs to the neighboring set $N_{set(i)}$ of node i . This approach allows GNN to selectively filter out non-neighboring node information and focus solely on computing the importance of nodes $j \in N_{set(i)}$. It is worth noting that in the TSP graph, all nodes are connected, implying that the neighboring set $N_{set(i)}$ of each node encompasses all the other nodes except itself. To expedite the model's training process, we select the top $\frac{n}{k}$ -nearest nodes as the neighbors of node i if n exceeds the threshold k . Finally, we compute the node features at the subsequent layer as follows:

$$v_i^l = \text{BN}(\left(\sum_j^n \alpha_{i,j}^l \odot v_j^{l-1}\right) + v_i^{l-1}), v_i^l \in \mathbb{R}^{n \times h}, \quad (9)$$

where BN denotes Batch Normalization [52].

2) **Edge**: The conventional approach for transferring edge feature information aggregates adjacent edges' features to update each edge's attributes [53]. However, in the TSP graph, all nodes are connected to each other. Hence, it is challenging to efficiently identify the adjacent edges. One of the promising strategies to address this issue is to utilize the information from the nodes at both ends of each edge to update its features. To accomplish this, we employ a single-layer feedforward NN with a trainable weight matrix and a bias term, which operates on all nodes, and compute their contribution C to the edge's features as follows:

$$C_{i,j}^l = v_1^l \oplus v_2^l, C_{i,j}^l \in \mathbb{R}^{n \times h \times h}, \quad (10)$$

$$v_1^l = \mathbf{W}_{e1}^l v_i^l + \mathbf{b}_{1i}^l, v_1^l \in \mathbb{R}^{n \times h \times 1}, \quad (11)$$

$$v_2^l = \mathbf{W}_{e2}^l v_j^l + \mathbf{b}_{2j}^l, v_2^l \in \mathbb{R}^{n \times 1 \times h}, \quad (12)$$

where \oplus denotes the addition operation with broadcasting. After computing each node's contribution to the edge features, we aggregate these contributions and apply the Sigmoid activation function σ_3 to compute the edge features at the subsequent layer as follows:

$$e_{i,j}^l = \text{BN}(\sigma_3(C_{i,j}^l + \mathbf{W}_{ee}^l e_{i,j}^{l-1} + \mathbf{b}_{i,j}^l) + e_{i,j}^{l-1}), e_{i,j}^l \in \mathbb{R}^{n \times n \times h}, \quad (13)$$

$$\sigma_3(z) = \frac{1}{1 + e^{-z}}. \quad (14)$$

3) **Starting symbol**: For the transfer of the starting symbol feature information, we introduce a virtual node $v_h \in \mathbb{R}^{1 \times h}$, which is randomly initialized and does not belong to the node set V (but virtually match to one node in V). This virtual node employs the self-attention mechanism [43] to learn and ultimately identify the most promising starting node in TSP solutions. Self-attention is a powerful technique used in conventional models [16] to map a query and a set of key-value pairs to an output. In this study, we leverage self-attention to interactively update the starting symbol's features by aggregating all features of each node. Specifically, we

define the query as the features of the starting symbol v_h and the key and value as the features of node v , as follows:

$$q^l = \mathbf{W}_q^l v_h^{l-1}, q^l \in \mathbb{R}^{1 \times h}, \quad (15)$$

$$K_i^l = \mathbf{W}_k^l v_i^l, K_i^l \in \mathbb{R}^{n \times h}, \quad (16)$$

$$V_i^l = \mathbf{W}_v^l v_i^l, V_i^l \in \mathbb{R}^{n \times h}, \quad (17)$$

where v_h^0 denotes the initial features of the starting symbol, which is equal to v_h . The starting symbol's features at the subsequent layer are given as:

$$v_h^l = \text{BN}\left(\sum_i^n \sigma_1(q^l K_i^{lT}) \odot V_i^l + v_h^{l-1}\right), v_h^l \in \mathbb{R}^{1 \times h}. \quad (18)$$

In the last layer of the GNN, the starting symbol acquires the probability of each node in V being the starting node by querying all nodes as follows:

$$\beta = \sigma_1(q K^T), \beta \in \mathbb{R}^{1 \times n}, \quad (19)$$

$$q = \mathbf{W}_q^{N_g} v_h^{N_g-1}, q^{N_g} \in \mathbb{R}^{1 \times h}, \quad (20)$$

$$K = \mathbf{W}_k^{N_g} v^{N_g}, K \in \mathbb{R}^{n \times h}, \quad (21)$$

where β denotes the probability distribution of n nodes as the starting node in TSP solutions. We use β to determine the pointer indicating where to initiate the decoding (see (26)) and let it be one model output.

The final component of NAR4TSP comprises N_f FC layers, which transform the edge features to prediction scores for the edges' likelihood of being selected in the TSP tour. Specifically, we use the edge features $e_{i,j}^{N_g}$ as the embedding of the edge at the first FC layer as follows:

$$A^0 = e_{i,j}^{N_g}, A^0 \in \mathbb{R}^{n \times n \times h}. \quad (22)$$

We then use the ReLU activation function σ_4 to compute the edge embedding at the subsequent layer as follows:

$$A^l = \sigma_4(\mathbf{W}_f^l A^{l-1} + \mathbf{b}_f^l), A^l \in \mathbb{R}^{n \times n \times h}, \quad (23)$$

$$\sigma_4(z) = \max(0, z), \quad (24)$$

where $l \in \{1, 2, 3, \dots, N_f - 1\}$ denotes the FC layer's index. The forward pass of the last layer is defined as follows:

$$A = \mathbf{W}_f^{N_f} A^{N_f-1} + \mathbf{b}_f^{N_f}, A \in \mathbb{R}^{n \times n \times 1}. \quad (25)$$

Finally, the model compresses the third axis to obtain the two-dimensional matrix of edge scores $A \in \mathbb{R}^{n \times n}$. This matrix A denotes the tightness of links between n nodes and is the other model output (other than the starting-node pointer).

C. Decoding Process of NAR4TSP

In the decoding process of the conventional NAR models [12], [13], the starting position for inference is typically set as the node indexed at 1. In contrast, we deem that selecting the starting position in a data-driven manner is more practical than always using a predetermined index as the starting position. This is the motivation of our design of the starting symbol in the GNN. Note that the starting position in this context refers to the index of a node, from which the model should start

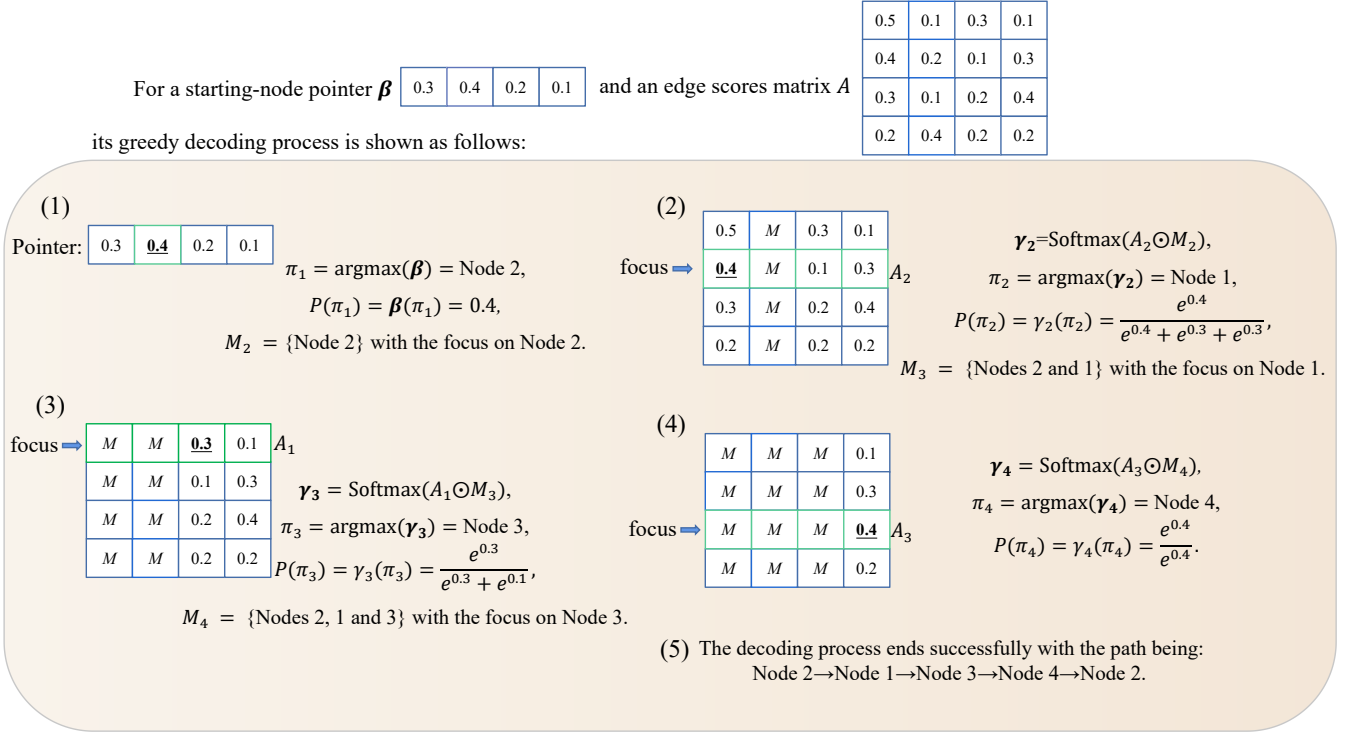


Fig. 2. An illustration of the decoding process of NAR4TSP using greedy search, assuming there are four nodes in the graph.

the decoding process. It does not mean that the tour has to start from this node. After the decoding process completes, one may always start the TSP tour from the node indexed at 1 or from any other predetermined node.

Fig. 2 shows an example of the decoding process of NAR4TSP using greedy search. To obtain a feasible TSP solution π from the output of NAR4TSP, i.e., a matrix of edge scores A and a starting-node pointer β , we incorporate the sequential constraints of TSP to decode them using the greedy search algorithm. Specifically, we start by generating the starting node as follows:

$$\pi_1 = \operatorname{argmax}(\beta). \quad (26)$$

Then, we apply the Softmax activation function σ_2 to normalize the edge scores, representing the tightness of the node links. We compute the probability distribution of the subsequent node by masking the probability of already visited nodes as follows:

$$\gamma_i = \sigma_2 \left(A_{i,j} \odot \begin{cases} -\infty, & \text{if node } j \in M_i, \\ 1, & \text{otherwise,} \end{cases} \right), \gamma_i \in \mathbb{R}^{1 \times n}, \quad (27)$$

where $i \in \{2, 3, \dots, n\}$, $A_{i,j}$ denotes the element value in the i th row and j th column of A , representing the tightness of the link between nodes i and j , and set M_i consists of all visited nodes, i.e., $\pi_1, \pi_2, \dots, \pi_{i-1}$. Finally, we obtain the sequence of the remaining nodes by adopting the greedy search algorithm as follows:

$$\pi_i = \operatorname{argmax}(\gamma_i). \quad (28)$$

More advanced sampling methods, such as beam search, are commonly used in solving TSPs [12], [16]. Beam search

is a breadth-first search method that operates within a limited width, denoted as B . This method commences its exploration from initial candidates (e.g., the starting node) and incrementally expands the tours by evaluating B potential successors. It selectively retains the top- B tours with the highest scores at each step, determined by their cumulative logarithmic probabilities. Greedy search is a special case of beam search with the width of 1. From the perspective of dynamic programming, setting B to $n \cdot 2^n$ guarantees optimal results [35], but selecting a small value of B greatly alleviates computational cost, albeit with possible degradation on performance. When using beam search, AR models exhibit limited search parallelism, because they require multiple probability distribution computations in each decoding stage [15], [16]. In contrast, NAR models such as NAR4TSP only perform search in the model output without multiple computations, significantly reducing the inference time [12], [13]. The time efficiency of NAR4TSP is further demonstrated with experimental results in Section IV-B.

D. Enhanced Reinforcement Learning Strategy of NAR4TSP

RL-based TSP solvers aim to minimize the overall length of all edges in a TSP tour. For a given TSP instance o , the loss function used for training is the overall tour length $L(\pi)$ of the current TSP solution:

$$\mathcal{L}(\theta|o) = \mathbb{E}_{P_\theta}[L(\pi)], \quad (29)$$

where P_θ denotes the policy parameterized by θ and the gradient of (29) can be computed as follows based on the well-known REINFORCE algorithm [54]:

$$\nabla \mathcal{L}(\theta|o) = \mathbb{E}_{P_\theta}[L(\pi) - L(b(o))] \nabla \log P_\theta(\pi|o), \quad (30)$$

where $P_\theta(\pi|o)$ denotes the probability of the TSP tour π based on the policy P_θ and $b(o)$ denotes the tour baseline for the TSP instance o .

A good baseline can reduce the gradients' variance, thereby accelerate the model's learning process [54]. Conventional models [15], [16] employ the self-critical RL strategy [18] consisting of two sub-modules with an identical architecture and initial parameters. Specifically, one sub-module predicts the tour π for training, while the other estimates the baseline $b(o)$. During training, these two sub-modules use different sampling methods: Bernoulli sampling for the prediction sub-module and greedy search for the baseline sub-module. After multiple training iterations, if the prediction sub-module outperforms the baseline sub-module, the latter adopts the parameters of the former to obtain a better baseline $b(o)$.

Although we employ RL to train our NAR model as well, different from the commonly adopted self-critical RL strategy, our proposed RL strategy in NAR4TSP takes advantage of the one-shot nature of NAR models. Specifically, our enhanced RL strategy only uses one training sub-module that directly utilizes both Bernoulli sampling and greedy search on the model's output to obtain the prediction π and the baseline $b(o)$, respectively. This approach eliminates the need for an additional sub-module, reducing required computational resources (see Section IV-D). In the following paragraphs, we present a comprehensive and detailed introduction to our enhanced RL strategy.

1) **State**: The state s_t , where $t \in \{0, 1, \dots, n\}$, is defined as the set of all previously visited nodes:

$$s_t = \begin{cases} \{\emptyset\}, & \text{if } t = 0, \\ \{\pi_1, \pi_2, \dots, \pi_t\}, & \text{otherwise.} \end{cases} \quad (31)$$

2) **Action**: The action a_t is defined as the node to be selected at time t :

$$a_t = \begin{cases} \pi_{t+1}, & \text{if } t < n, \\ \pi_1, & \text{otherwise.} \end{cases} \quad (32)$$

3) **Reward**: The reward $r(s_t, a_t)$ is defined as the negative cost (i.e., length in this paper, see (1)) incurred from taking action a_t from state s_t :

$$r(s_t, a_t) = \begin{cases} 0, & \text{if } t = 0, \\ -x_{a_{t-1}, a_t}^e, & \text{otherwise.} \end{cases} \quad (33)$$

4) **Policy**: The policy $P_\theta(s_t)$ generates a probability distribution for the unvisited nodes based on the state s_t . It is worth noting that our policy differs from that of the conventional RL-based AR models [15], [16] which requires interactions with the NN's weight each time when the probability distribution for the next node is obtained, i.e., each node is generated using a computationally intensive NN. Our policy only needs to access the GNN's weight once, retrieve the output pointer and the edge scores matrix at each stage t , and subsequently determine which node to visit next until a complete TSP solution is produced. We deem both advantageous properties of NAR4TSP, namely lesser number of RL sub-modules in use and much lesser number of required interactions between

Algorithm 1 The training process of NAR4TSP.

Input: the number of epochs n_e , steps per epoch n_s , validation set size n_v , and batch size n_{bs}

- 1: Initialize θ , set $L_{tmp} \leftarrow \infty$, and obtain validation set o_{va} by randomly generating n_v TSP instances
- 2: **for** $epoch$ in $1, \dots, n_e$ **do**
- 3: **for** $step$ in $1, \dots, n_s$ **do**
- 4: $o_{tr} \leftarrow$ Randomly generate n_{bs} TSP instances
- 5: $\beta, A \leftarrow \mathbf{model}(o_{tr}, \theta)$
- 6: $\pi(o_{tr}), P_\theta(\pi|o_{tr}) \leftarrow$ Bernoulli sample (β, A)
- 7: $b(o_{tr}) \leftarrow$ Greedy search (β, A)
- 8: $\nabla \mathcal{L} \leftarrow (L(\pi(o_{tr})), L(b(o_{tr})), P_\theta(\pi|o_{tr}))$ (see (36))
- 9: $\theta \leftarrow \text{Adam}(\theta, \nabla \mathcal{L})$
- 10: **end for**
- 11: $\beta, A \leftarrow \mathbf{model}(o_{va}, \theta)$
- 12: $\pi(o_{va}) \leftarrow$ Greedy search (β, A)
- 13: **if** $\text{mean}(L(\pi(o_{va}))) < L_{tmp}$ **then**
- 14: $L_{tmp} \leftarrow \text{mean}(L(\pi(o_{va})))$
- 15: Save (θ)
- 16: **end if**
- 17: **end for**

the policy and the external NNs, the key enhancement of our RL strategy used in NAR4TSP.

Upon visiting all nodes, the policy is then updated by maximizing the cumulative rewards $\sum_{t=0}^n r(s_t, a_t)$, i.e., $-L(\pi)$ (see (29)).

When given a TSP instance o , NAR4TSP decodes its corresponding output to obtain a TSP tour π , where the probability of selecting the subsequent node at each stage is determined as follows:

$$P_\theta(a_t|s_t) = \begin{cases} \beta(\pi_1), & \text{if } t = 0, \\ \gamma_{t+1}(\pi_{t+1}), & \text{if } 0 < t < n, \\ 1, & \text{if } t = n, \end{cases} \quad (34)$$

where $\beta(\pi_1)$ and $\gamma_t(\pi_t)$ denote the probability of choosing the first node and the t th node in the TSP solution, respectively. Subsequently, the probability of the TSP tour π is computed based on the chain rule as follows:

$$P_\theta(\pi|o) = \prod_{t=0}^n P_\theta(a_t|s_t). \quad (35)$$

Furthermore, we adopt the central self-critical from [26] to accelerate model convergence. Thus, the exact value of (30) is obtained as follows:

$$\begin{aligned} \nabla \mathcal{L}(\theta|s) &= \frac{1}{n_{bs}} \sum^{n_{bs}} [L(\pi) - L(b(o)) + \omega] \\ &\quad \cdot \nabla (\log \beta(\pi_1) + \sum_{i=2}^n \log \gamma_i(\pi_i)), \end{aligned} \quad (36)$$

$$\omega = \frac{1}{n_{bs}} \sum^{n_{bs}} [L(\pi) - L(b(o))], \omega \in \mathbb{R}^1, \quad (37)$$

where n_{bs} denotes the value of batch size.

TABLE II
PERFORMANCE OF NAR4TSP WITH COMPARISONS WITH BENCHMARKING METHODS ON TSP50 AND TSP100 INSTANCES

category	method	type	N_{paras}	TSP50				TSP100			
				average length \downarrow	optimality gap \downarrow	S time (sec) \downarrow	T time (sec), n_{bs} \downarrow	average length \downarrow	optimality gap \downarrow	S time (sec) \downarrow	T time (sec), n_{bs} \downarrow
Conventional algorithms	Concorde (2007) [14]	exact solver	N.A.	5.689	0.00%	0.035	3.63×10^2 , 1	7.765	0.00%	0.165	1.45×10^3 , 1
	Nearest Insertion	heuristic	N.A.	6.978	22.66%	0.020	2.04×10^1 , 1	9.676	70.07%	0.044	4.36×10^1 , 1
	Fastest Insertion	heuristic	N.A.	5.999	5.47%	0.024	2.41×10^1 , 1	8.347	7.50%	0.059	5.82×10^1 , 1
Neural improvement algorithms	Wu <i>et al.</i> , $T=1000$ (2022) [23]	RL, heuristic	-	5.740	0.89%	-	-	8.010	3.16%	-	-
	Wu <i>et al.</i> , $T=3000$ (2022) [23]	RL, heuristic	-	5.710	0.36%	-	-	7.910	1.87%	-	-
	Costa <i>et al.</i> , $T=1000$ (2021) [24]	RL, heuristic	1.34M	5.735	0.81%	11.291	1.26×10^3 , 500	7.851	1.10%	12.981	2.20×10^3 , 128
	Costa <i>et al.</i> , $T=2000$ (2021) [24]	RL, heuristic	1.34M	5.718	0.52%	22.413	2.58×10^3 , 500	7.820	0.71%	26.322	4.32×10^3 , 128
End-to-end models with greedy search	Vinyals <i>et al.</i> (2015) [19]	SL, AR	-	7.660	34.64%	-	-	-	-	-	-
	Bello <i>et al.</i> (2017) [20]	RL, AR	-	5.950	4.59%	-	-	8.300	6.89%	-	-
	Khalil <i>et al.</i> (2017) [21]	RL, AR	-	5.990	5.29%	-	-	8.310	7.02%	-	-
	Deudon <i>et al.</i> (2018) [22]	RL, AR	-	5.920	4.06%	-	-	8.420	8.44%	-	-
	Kool <i>et al.</i> (2019) [15]	RL, AR	0.71M	5.783	1.65%	0.079	4.68×10^0 , 500	8.097	4.28%	0.154	1.88×10^1 , 128
	Bresson and Laurent (2021) [16]	RL, AR	1.41M	5.707	0.32%	0.146	4.95×10^0 , 500	7.876	1.43%	0.277	2.24×10^1 , 128
	Jung <i>et al.</i> (2023) [17]	RL, AR	1.43M	5.754	1.13%	0.163	5.16×10^0 , 500	7.985	2.83%	0.240	2.38×10^1 , 128
	Joshi <i>et al.</i> (2019) [13]	SL, NAR	11.05M	5.870	3.18%	0.048	8.02×10^1 , 250	8.410	8.31%	0.090	3.70×10^2 , 64
	NAR4TSP (ours)	RL, NAR	0.91M	5.752	1.11%	0.022	9.49×10^0 , 500	7.899	1.74%	0.034	3.58×10^1 , 128
	End-to-end models with beam search	Kool <i>et al.</i> , $B=1280$ (2019) [15]	RL, AR	0.71M	5.716	0.47%	0.132	1.07×10^3 , 1	7.939	2.24%	0.306
Kool <i>et al.</i> , $B=2560$ (2019) [15]		RL, AR	0.71M	5.713	0.42%	0.192	1.51×10^3 , 1	7.931	2.14%	0.462	4.50×10^3 , 1
Bresson and Laurent, $B=100$ (2021) [16]		RL, AR	1.41M	5.692	0.05%	0.169	3.08×10^2 , 150	7.818	0.68%	0.294	8.73×10^2 , 80
Bresson and Laurent, $B=1000$ (2021) [16]		RL, AR	1.41M	5.691	0.04%	0.280	1.76×10^3 , 15	7.803	0.49%	0.781	6.48×10^3 , 5
Jung <i>et al.</i> , $B=1000$ (2023) [17]		RL, AR	1.43M	5.697	0.09%	0.241	1.16×10^3 , 20	7.861	1.24%	0.732	3.88×10^3 , 10
Joshi <i>et al.</i> , $B=1280$ (2019) [13]		SL, NAR	11.05M	5.710	0.36%	0.073	1.45×10^2 , 250	7.920	2.00%	0.188	6.31×10^2 , 64
Joshi <i>et al.</i> , $B=1280$ (2019) [13]		SL, NAR	11.05M	5.700	0.19%	4.295	1.98×10^3 , 250	7.880	1.48%	8.974	4.57×10^3 , 64
NAR4TSP, $B=100$ (ours)		RL, NAR	0.91M	5.712	0.40%	0.038	1.05×10^1 , 500	7.845	1.02%	0.065	4.01 $\times 10^3$, 128
NAR4TSP, $B=1000$ (ours)		RL, NAR	0.91M	5.705	0.28%	0.047	1.86×10^1 , 500	7.827	0.80%	0.113	7.26 $\times 10^3$, 128

Symbol T denotes the number of iterations in the improvement process; symbol B^* denotes the beam search with the shortest tour heuristic used in [13]; “optimality gap” indicates the relative difference in “average length” between each model and Concorde; “S time” indicates the inference time of solving a single TSP instance on average; and “T time, n_{bs} ” indicates the inference time with batch size n_{bs} on all the 10,000 testing TSP instances. Because of the end-to-end models’ parallel processing nature, the reported value of “T time” does not equal to the multiplication of the corresponding “S time” and the total number of instances.

The overall training process of NAR4TSP is outlined in Algorithm 1. Our implementation of NAR4TSP (in PyTorch) is accessible online¹.

IV. EXPERIMENTAL RESULTS

This section presents a set of comprehensive evaluations of NAR4TSP. We start by providing an overview of the hyper-parameter settings of NAR4TSP, followed by an assessment of the model’s performance in terms of solution quality, inference ability, and generalization ability. Next, we illustrate the decoding process and the overall path planning of NAR4TSP through visualizations. Finally, we conduct ablation studies on the unique GNN architecture of NAR4TSP and the enhanced RL strategy proposed in this paper.

A. Hyper-parameter Configuration

For all experiments conducted in this paper, we consistently set the hyper-parameters of NAR4TSP. Specifically, NAR4TSP consists of $N_g = 6$ GNN modules and $N_f = 2$ FC layers, with a hidden dimension of 128 for each layer and the multi-head attention number of 8, following [16]. The trade-off parameter δ in (4) is set to 0.2, following [51]. To determine a node’s neighbors, we consider the top $\frac{n}{5}$ -nearest nodes, following [13]. The validation set size n_v is set to 10,000. Each epoch consists of $n_s = 2,500$ batches of $n_{bs} = 64$ instances, with all training instances being generated randomly on the fly, following [15], [16]. The number of training epochs varies based on the TSP size, with $n_e = 1,000$ and $n_e = 2,000$ epochs used for $n = 50$ and $n = 100$, respectively, following [16]. We use Adam [55] as the optimizer, with a constant learning rate

of $1e-4$ for simplification, despite that we recommend fine-tuning the learning rate (e.g., learning rate decay) for faster convergence. All experiments were conducted on a computer equipped with an Intel(R) Core(TM) i5-11400F CPU and an NVIDIA RTX 3060Ti GPU.

B. Performance of NAR4TSP

We conduct comprehensive experiments to assess the performance of NAR4TSP in three key aspects, namely solution quality, inference latency, and generalization ability.

1) **Solution quality:** We follow the convention and report the performance of NAR4TSP for solving 10,000 two-dimensional TSP instances [13], [15], [16], where all test instances are randomly generated by sampling the node locations based on the unit uniform distribution. Table II presents the performance of our model compared to the benchmarking methods on 10,000 test instances of TSP50 and TSP100. The methods compared in Table II are categorized into four groups, namely conventional algorithms (including exact solver and heuristics), neural improvement algorithms, end-to-end models with greedy search, and end-to-end models with beam search. To ensure a fair comparison on the inference time on all 10,000 test instances, we intend to maintain an equal batch size n_{bs} for all NN-based models. But limited by the GPU memory (8GB), three models [15]–[17] have to be run with smaller batch sizes when using beam search, and one [13] has to use a smaller batch size than other models due to its large number of learnable parameters.

Table II shows that models employing beam search outperform those using greedy search due to the wider search range it offers for potential solutions. Nonetheless, the utilization of beam search significantly impacts the performance of AR models [15]–[17], particularly in terms of inference time and

¹URL: <https://github.com/xybFight/NAR4TSP>

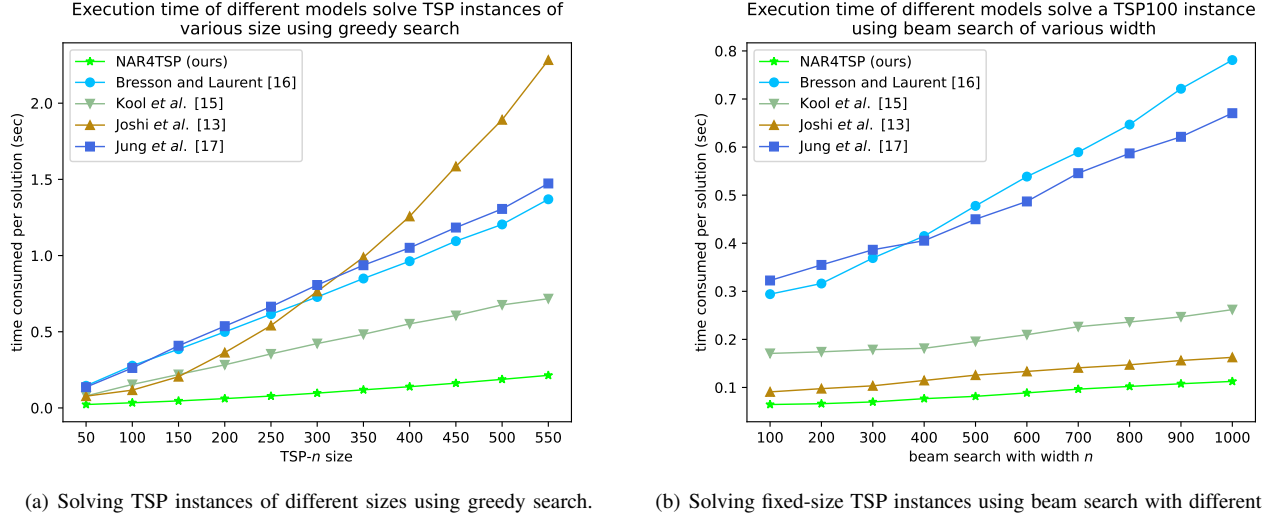


Fig. 3. Comparison on the inference time between our model and SOTA models.

parallel processing capability (i.e., the ability to simultaneously process n_{bs} input instances). In contrast, NAR models, including NAR4TSP, remain largely unaffected. Despite the one-shot nature of NAR decoding [25], NAR4TSP achieves competitive solution quality compared to all benchmarking NN-based models, with the exception of only one AR model [16]. This could be attributed to the fact that the model in [16] considers the contribution of all previously visited nodes when determining the next node for travel. However, such an approach undoubtedly increases the computational burden. Remarkably, compared to the best solution quality obtained by [16] with beam search width $B = 1,000$, NAR4TSP demonstrates significant advantages in terms of the inference time, with $\frac{1.76 \times 10^3}{1.86 \times 10^1} \approx 94$ times improvement on 10,000 TSP50 instances and $\frac{6.48 \times 10^3}{7.26 \times 10^1} \approx 89$ times improvement on 10,000 TSP100 instances, while only experiencing a slight reduction in solution quality ($1 - \frac{5.691}{5.705} \approx 0.24\%$ and $1 - \frac{7.803}{7.827} \approx 0.30\%$, respectively). Compared to another SOTA NAR model [13], NAR4TSP demonstrates notable advancements while utilizing a significantly smaller number of learnable parameters, i.e., $\frac{11.05}{0.91} \approx 12.14$ times. Specifically, NAR4TSP exhibits a remarkable $\frac{1.45 \times 10^2}{1.86 \times 10^1} \approx 7.8$ times improvement in inference time and a slight yet noteworthy $\frac{5.710}{5.705} - 1 \approx 0.08\%$ enhancement in solution quality when solving 10,000 TSP50 instances using beam search. Similarly, when solving 10,000 TSP100 instances, NAR4TSP exhibits $\frac{6.31 \times 10^2}{7.26 \times 10^1} \approx 8.7$ times improvement in inference time and $\frac{7.920}{7.827} - 1 \approx 1.19\%$ improvement in solution quality. Furthermore, NAR4TSP outperforms all the other NN-based methods in terms of the averaged inference time, highlighting its ability to produce high-quality solutions with low latency.

2) **Inference latency:** To comprehensively evaluate the inference speed of NAR4TSP, we compare the time taken by NAR4TSP and four SOTA models [13], [15]–[17] for solving TSP instances of varying sizes and beam widths. Figs. 3(a) and 3(b) illustrate the inference time taken by these models when using greedy search for TSP instances of different sizes

and beam search with different widths for a fixed-size TSP instance, respectively.

Fig. 3 illustrates that NAR4TSP outperforms the other SOTA models in terms of inference speed. The disparity in inference time between NAR4TSP and the other models becomes increasingly prominent as the number of nodes and beam width increase. These experimental results demonstrate that our NAR4TSP model is much more applicable to real-time TSP tasks due to its low inference latency.

3) **Generalization ability:** The ability to generalize effectively across TSP instances in different sizes is a highly desirable characteristic for NN-based models to solve CO problems [25]. Notably, NAR4TSP shares parameters across all nodes, thus enabling it to remain robust to variations in the number of nodes. This property of NAR4TSP allows the application of a pre-trained model to solve TSP instances of different sizes.

To assess the generalization ability of each model, we compare NAR4TSP with four SOTA models [13], [15]–[17]. Table III presents the performance of the models trained using TSP50 instances and applied to solve 10,000 TSP100 and TSP200 (TSP with 200 nodes) instances. Similarly, Table IV demonstrates the performance of the models trained using TSP100 instances and applied to solve 10,000 TSP50 and TSP200 instances. We exclude the TSP200-trained models from the generalization comparisons due to the substantial training time and failure to converge, as observed in two SOTA models [13], [15]. The experimental results presented in Tables III and IV demonstrate that NAR4TSP and three AR models [15]–[17] perform well, while the other model [13] does not. The plausible reason is overfitting that the model [13] uses an excessive number of parameters (over 11 million) to memorize TSP training patterns, but the learned policy is still unable to generalize beyond the training sizes [25]. Importantly, NAR4TSP exhibits superior generalization ability compared to all the other SOTA models [13], [15]–[17]. Furthermore, the results presented in Tables III and IV indicate

TABLE III
GENERALIZATION PERFORMANCE OF APPLYING MODELS TRAINED USING
TSP50 INSTANCES ONTO TSP100 AND TSP200 INSTANCES

model trained using TSP50 instances	type	beam width	TSP100		TSP200	
			average length \downarrow	optimality gap \downarrow	average length \downarrow	optimality gap \downarrow
Kool <i>et al.</i> (2019) [15]	RL, AR	1	8.144	4.88%	12.142	13.39%
		1280	7.981	2.78%	12.904	20.49%
		2560	7.966	2.59%	12.847	19.96%
Bresson and Laurent (2021) [16]	RL, AR	1	8.023	4.11%	12.966	21.08%
		100	7.929	3.12%	12.930	20.75%
		1000	7.906	1.82%	12.948	20.91%
Jung <i>et al.</i> (2023) [17]	RL, AR	1	8.166	5.17%	12.435	16.13%
		1000	7.990	2.90%	12.224	14.16%
Joshi <i>et al.</i> (2019) [13]	RL, NAR	1	13.383	72.35%	21.688	102.54%
		1280	12.222	57.40%	21.393	99.79%
NAR4TSP (ours)	RL, NAR	1	8.051	3.68%	11.828	10.45%
		100	7.961	2.20%	11.617	8.49%
		1000	7.898	1.72%	11.532	7.69%

TABLE IV
GENERALIZATION PERFORMANCE OF APPLYING MODELS TRAINED USING
TSP100 INSTANCES ONTO TSP50 AND TSP200 INSTANCES

model trained using TSP100 instances	type	beam width	TSP50		TSP200	
			average length \downarrow	optimality gap \downarrow	average length \downarrow	optimality gap \downarrow
Kool <i>et al.</i> (2019) [15]	RL, AR	1	5.935	4.32%	11.569	8.04%
		1280	5.821	2.34%	11.424	6.70%
		2560	5.816	2.23%	11.400	6.46%
Bresson and Laurent (2021) [16]	RL, AR	1	6.214	9.22%	11.419	6.65%
		100	5.860	3.00%	11.278	5.33%
		1000	5.784	1.67%	11.240	4.97%
Jung <i>et al.</i> (2023) [17]	RL, AR	1	5.867	3.13%	11.576	8.10%
		1000	5.751	1.08%	11.387	6.34%
Joshi <i>et al.</i> (2019) [13]	RL, NAR	1	7.696	35.25%	16.827	57.14%
		1280	7.422	30.44%	16.383	53.00%
NAR4TSP (ours)	RL, NAR	1	5.808	2.09%	11.200	4.59%
		100	5.739	0.88%	11.083	3.50%
		1000	5.724	0.62%	11.037	3.07%

that the generalization performance of NAR4TSP improves as the size of the TSP instances used for training increases, which is consistent with the commonsense that if the model is trained using complex examples, it should perform well on less complex ones.

Nonetheless, in Tables III and IV, the node coordinates in the test instances are all sampled based on the unit uniform distribution, which is consistent with the training data. We further evaluate the generalization ability of NAR4TSP and three SOTA AR models [15]–[17] using the widely adopted TSPLIB² dataset. TSPLIB is a repository of TSP instances widely used to assess the effectiveness of algorithms for solving TSPs [40], [50]. To this end, we randomly select 25 real-world TSP instances of different sizes (ranging from 51 to 575 nodes) from the TSPLIB dataset as test instances. Unlike the training instances where the node coordinates are bounded between 0 and 1, the node coordinates of the real-world instances in TSPLIB are integers that span from one to thousands and in some cases, even negative values. To maximally simulate the unknown real-world scenarios, we refrain from applying any preprocessing methods, such as normalization, rotation, or transformation, to the test instances. Instead, we straightforwardly apply the models trained using the TSP50 instances to solve the 25 real-world instances. This setting is widely known as zero-shot generalization [25]. A model capable of generating good solutions in such cases signifies its ability to recognize and learn the underlying patterns and insights of TSPs, making it suitable for diverse

applications, as opposed to superficial pattern recognition [25].

As shown in Table V, the three SOTA models [15]–[17] exhibit unsatisfactory results. Although increasing the beam width B generally improves the solution quality by preserving the top- B candidate solutions with the highest probability, the model [16] only shows a $1 - \frac{167.08\%}{176.58\%} \approx 5.37\%$ improvement in performance as B increases from 1 to 1000, while the performance of the other two models [15], [17] even decreases by $\frac{701.59\%}{455.92\%} - 1 \approx 53.88\%$ and $\frac{655.44\%}{475.11\%} - 1 \approx 37.95\%$, respectively. This finding indicates that these models have difficulties in handling TSP cases formulated differently from the training instances. In contrast, NAR4TSP outperforms these models by showcasing a $1 - \frac{11.51\%}{19.26\%} \approx 40.25\%$ improvement in solution quality when the beam width B increases from 1 to 1000. Furthermore, NAR4TSP exhibits significantly lower computation time, accounting for only $\frac{0.162}{3.573} \approx 4.53\%$ of the total time taken by [16], $\frac{0.162}{1.331} \approx 12.17\%$ of the total time taken by [15], and $\frac{0.162}{2.485} \approx 6.52\%$ of the total time taken by [17]. This finding highlights the remarkable time efficiency of our NAR4TSP model.

Furthermore, we preprocess the 25 real-world TSP instances by normalizing their node coordinates and subsequently compare the performance of NAR4TSP with the three SOTA models on the normalized TSP instances. The results, presented in the last two rows of Table V, indicate that NAR4TSP again outperforms the three SOTA models. Remarkably, NAR4TSP achieves better performance even without requiring instances normalization (optimality gap = 11.51% when $B = 1,000$) comparing to the three SOTA models with instances normalization, despite the significant improvement in solution quality attained by the latter after normalization.

C. Visualization of the Decoding Process and the Overall Path Planning of NAR4TSP

We employ two visualization methods to demonstrate the feasibility of implementing NAR4TSP in an end-to-end manner and the effectiveness of NAR4TSP, respectively.

Firstly, we visualize the decoding process of NAR4TSP using a randomly generated TSP5 (TSP with five nodes) instance as input. We depict the probability distribution of selecting the next node at each decoding stage. As shown in Fig. 4, our model produces a deterministic sequence by decoding a pointer and a matrix of edge scores, indicating its ability to learn an end-to-end mapping from the TSP information to the solution. Additionally, the heatmap of the score matrix A reveals that NAR4TSP goes beyond learning simple domain relations, such as the distance relationship between nodes. In this case, the diagonal elements are expected to consistently exhibit the largest values within their respective rows, because they represent the proximity of a node to itself, which should yield the highest similarity score among all nodes. However, it is worth noting that matrix A contains numerous elements with values surpassing those of the diagonal elements in their corresponding rows. This observation implies the existence of nodes that exhibit stronger connections to other nodes than to themselves, showcasing that our model has learned the intrinsic mapping relationships correctly.

²URL: <http://comopt.ifl.uni-heidelberg.de/software/TSPLIB95/>

TABLE V
ZERO-SHOT GENERALIZATION PERFORMANCE OF APPLYING MODELS TRAINED USING TSP50 INSTANCES ONTO 25 REAL-WORLD INSTANCES.

instance	Bresson and Laurent (2021) [16]				Kool <i>et al.</i> (2019) [15]				Jung <i>et al.</i> (2023) [17]				NAR4TSP (ours)			
	$B=1$		$B=1000$		$B=1$		$B=1000$		$B=1$		$B=1000$		$B=1$		$B=1000$	
	optimality gap ↓	time (sec) ↓	optimality gap ↓	time (sec) ↓	optimality gap ↓	time (sec) ↓	optimality gap ↓	time (sec) ↓	optimality gap ↓	time (sec) ↓	optimality gap ↓	time (sec) ↓	optimality gap ↓	time (sec) ↓	optimality gap ↓	time (sec) ↓
berlin52	93.56%	0.155	84.90%	0.283	222.32%	0.156	210.55%	0.188	267.37%	0.153	297.98%	0.394	30.51%	0.029	10.94%	0.040
ch130	190.07%	0.346	174.98%	1.271	608.59%	0.302	520.94%	0.572	623.57%	0.326	562.14%	1.122	19.81%	0.057	12.97%	0.094
ch150	187.71%	0.392	153.30%	1.681	765.45%	0.324	599.52%	0.746	720.82%	0.439	655.12%	1.450	14.90%	0.062	8.89%	0.111
d198	114.24%	0.527	111.65%	2.772	307.85%	0.480	884.74%	1.052	282.38%	0.573	995.16%	2.120	20.75%	0.086	15.67%	0.159
d493	181.97%	1.259	172.41%	15.816	226.12%	1.193	1106.16%	5.432	450.63%	1.331	583.17%	9.802	19.85%	0.287	14.98%	0.530
eil101	104.13%	0.232	95.41%	0.804	372.40%	0.233	345.98%	0.417	326.55%	0.300	407.15%	0.799	15.62%	0.055	11.58%	0.088
eil51	80.84%	0.118	64.51%	0.269	268.03%	0.141	217.18%	0.185	255.87%	0.155	242.72%	0.369	14.10%	0.033	3.72%	0.044
eil76	95.76%	0.184	87.36%	0.516	373.93%	0.183	269.14%	0.271	337.17%	0.230	345.17%	0.578	14.34%	0.045	9.83%	0.075
gil262	539.90%	0.674	506.75%	4.600	1022.72%	0.606	901.04%	1.858	939.61%	0.743	927.63%	3.333	22.96%	0.123	17.52%	0.236
kroA100	171.14%	0.273	156.50%	0.792	730.25%	0.219	516.93%	0.374	755.84%	0.296	751.52%	0.915	39.01%	0.047	16.16%	0.095
kroB150	186.67%	0.380	178.55%	1.655	713.21%	0.380	550.89%	0.795	941.20%	0.411	913.69%	1.400	20.17%	0.066	16.06%	0.109
kroD100	152.91%	0.259	143.06%	0.801	517.61%	0.251	397.31%	0.404	698.75%	0.274	583.41%	0.779	17.81%	0.061	11.30%	0.073
kroE100	160.57%	0.307	138.24%	0.810	704.46%	0.295	445.74%	0.400	770.32%	0.278	656.38%	0.820	19.06%	0.056	10.70%	0.074
lin105	207.39%	0.287	187.51%	0.868	649.11%	0.284	424.61%	0.431	225.33%	0.293	684.89%	0.851	12.90%	0.048	8.23%	0.082
lin318	301.79%	0.860	336.47%	6.848	538.74%	0.789	1110.76%	2.442	314.61%	0.862	661.62%	4.678	19.38%	0.158	15.33%	0.271
pcb442	308.81%	1.192	292.29%	12.484	910.06%	1.082	1186.35%	4.380	509.00%	1.244	863.51%	7.968	23.28%	0.249	16.24%	0.421
pr107	35.90%	0.280	28.14%	0.884	554.30%	0.374	670.63%	0.404	41.64%	0.307	606.72%	0.908	8.74%	0.045	6.49%	0.088
pr144	86.17%	0.382	66.82%	1.551	428.35%	0.349	889.62%	0.613	612.85%	0.414	999.26%	1.324	7.34%	0.061	6.86%	0.104
pr226	141.45%	0.639	157.34%	3.594	80.08%	0.516	1435.42%	1.394	862.92%	0.647	1524.86%	2.630	29.05%	0.102	8.45%	0.187
pr264	118.66%	0.688	111.44%	4.875	314.77%	0.614	1663.57%	1.780	1007.34%	0.750	1832.27%	3.332	16.75%	0.124	10.58%	0.210
pr76	136.02%	0.208	117.72%	0.483	221.80%	0.209	307.85%	0.262	168.01%	0.232	335.40%	0.578	17.15%	0.038	5.05%	0.058
rat195	212.04%	0.503	219.91%	2.600	146.81%	0.480	727.44%	1.029	73.48%	0.568	83.81%	2.062	18.43%	0.118	12.55%	0.152
rat575	337.21%	1.511	346.37%	21.855	172.43%	1.366	1401.64%	7.223	158.16%	1.652	244.69%	12.642	24.76%	0.396	17.57%	0.627
rat99	161.02%	0.246	153.66%	0.770	136.68%	0.246	435.97%	0.391	120.64%	0.269	229.15%	0.788	17.53%	0.046	10.95%	0.074
st70	108.56%	0.204	91.82%	0.426	412.01%	0.176	319.66%	0.241	413.78%	0.181	398.52%	0.495	17.41%	0.033	9.14%	0.053
average	176.58%	0.484	167.08%	3.573	455.92%	0.450	701.59%	1.331	475.11%	0.517	655.44%	2.485	19.26%	0.097	11.51%	0.162
Normalized 25 instances																
average	24.05%	0.479	25.81%	3.461	17.46%	0.462	26.51%	1.322	15.26%	0.531	15.02%	2.662	16.29%	0.102	11.76%	0.169

Optimality gaps indicate length differences compared to the optimal solutions from TSPLIB. Time indicates inference time.

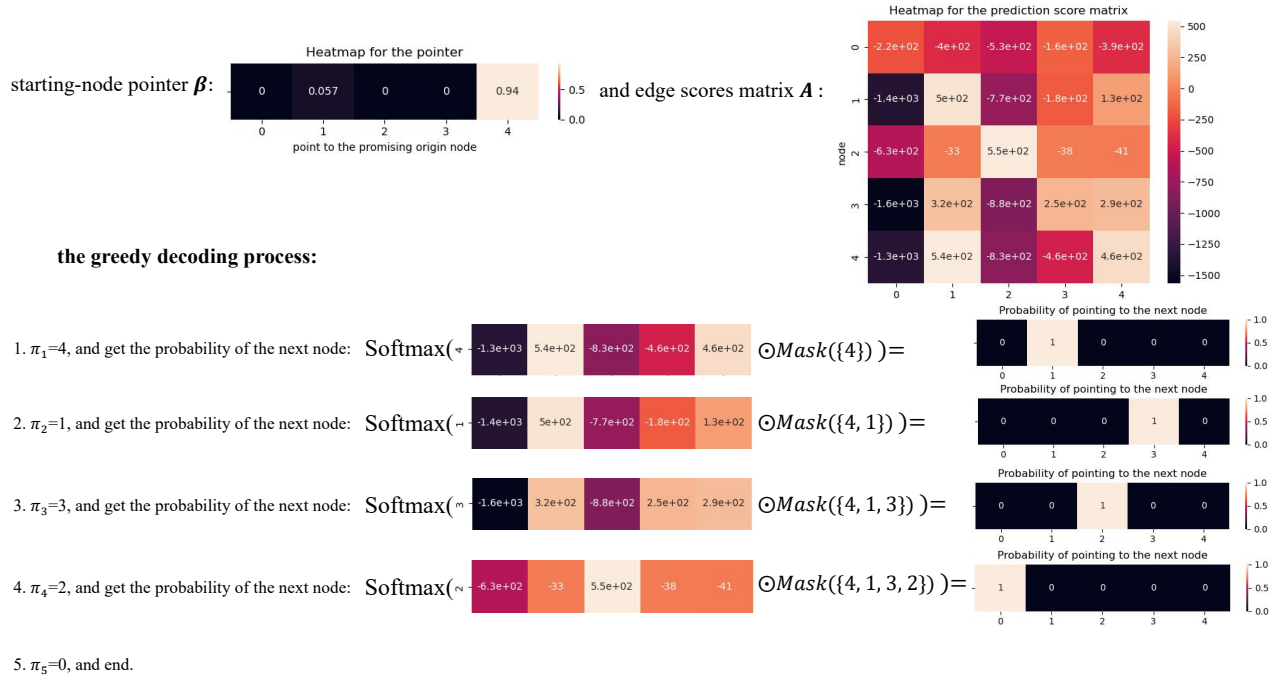


Fig. 4. Visualization of a TSP5 instance's greedy decoding process.

Secondly, we visualize the overall path planning of NAR4TSP by randomly selecting a set of TSP50 and TSP100 instances, respectively and comparing the solutions produced by NAR4TSP with greedy search and the optimal solution given by Concorde. As shown in Fig. 5, NAR4TSP yields on-par tour lengths comparing with those of Concorde, thus demonstrating the effectiveness of our model in solving TSPs.

D. Effectiveness of the Novel GNN Architecture and the Enhanced RL Strategy

In this subsection, we evaluate the effectiveness of the novel GNN architecture and the enhanced RL strategy proposed in this paper. Specifically, we use 10,000 TSP50 instances as the test set and systematically evaluate the performance by varying the components under investigation. Specifically, we conduct three ablation studies to evaluate the effectiveness of the GNN architecture. Firstly, we replace the proposed GNN architec-

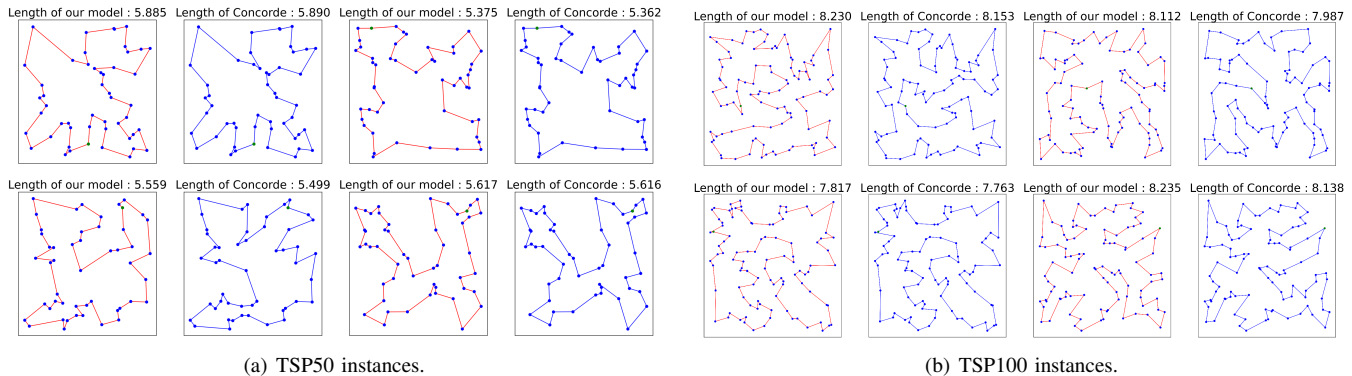


Fig. 5. Visualization of solutions produced by NAR4TSP using greedy search and Concorde, respectively.

TABLE VI
PERFORMANCE COMPARISON OF THE GCN OF [13] AND NAR4TSP

model architecture	N_{paras}	average length ↓	S time (sec) ↓	T time (sec), n_{bs} ↓
GCN used in [13]	11.05M	6.398	0.046	79.21, 250
GNN (ours)	0.91M	5.752	0.021	9.39, 500
GNN without the pointer mechanism	0.91M	6.117	0.020	9.21, 500
		5.748		
GNN with all nodes as the starting node	0.91M	7.466	0.029	19.14, 500
	min	6.671		
	max			
	mean			

ture with the GCN introduced in [13]. Secondly, we remove the pointer β from NAR4TSP and adopt the convention of [12], [13] to use the first node as the starting position for both training and testing. Thirdly, we employ an inference method akin to the one used in [56], selecting all nodes as the potential starting position for inference, which inevitably increases the computational cost and inference latency.

We present the ablation study results in Table VI. Firstly, although the architecture of [13] employs more learnable parameters than NAR4TSP, its average solution length on TSP50 is merely 6.398 (using greedy search). This represents a $\frac{6.398}{5.752} - 1 \approx 11.23\%$ decrease compared to NAR4TSP using our proposed GNN architecture, thus highlighting the effectiveness of the novel GNN architecture. Secondly, the absence of the pointer mechanism in NAR4TSP leads to a relative performance drop of $\frac{6.117}{5.752} - 1 \approx 6.34\%$ on the test set, underscoring the contribution of the learnable pointer. It is worth noting that even in the absence of the pointer mechanism, NAR4TSP achieves an average solution length that is on-par with that of the SOTA NAR model [13] along with a $\frac{8.02 \times 10^4}{9.21 \times 10^0} \approx 8.7$ -fold speed enhancement (see Table II). This result can be attributed to the well-designed GNN architecture that facilitates TSP representation extraction (see Section III-B). Thirdly, when each node is considered as the starting position, the minimum solution length is only $1 - \frac{5.748}{5.752} \approx 0.06\%$ better than the solution length derived based on the NAR4TSP’s determined pointer β . It is worth noting that the former must be less than or equal to the latter. Equality is only achieved when the starting node, associated with the solution having the minimum length in these 10,000 TSP instances, exactly matches the node indicated by the pointer β . Conversely, the mean solution length is $\frac{6.671}{5.752} - 1 \approx 15.97\%$ worse than the

TABLE VII
EFFECTIVENESS COMPARISON OF THE ORIGINAL RL STRATEGY AND OUR ENHANCED RL STRATEGY

strategy	GPU Memory usage (MB) ↓	training time per epoch (min) ↓	average length ↓
original RL	4906.95	12.27	5.780
enhanced RL (ours)	4465.12	9.71	5.752

solution length derived based on the NAR4TSP’s determined pointer β . These results demonstrate that the solution derived by pointer β closely approximates the optimal decision (i.e., the starting node associated with the solution has the minimum length). Moreover, there exists a significant gap of up to $\frac{7.466}{5.748} - 1 \approx 29.88\%$ between the solution lengths obtained using different starting nodes, underscoring the importance of selecting the appropriate one. This result further justifies our primary motivation behind the design of the starting-node pointer.

We further compare the performance of NAR4TSP utilizing our enhanced RL strategy with the original RL strategy used in conventional models [15], [16], [26]. As introduced in Section III-D, the original RL strategy uses two sub-modules with the identical architecture, while ours only uses one. As shown in Table VII, our enhanced RL strategy is more resource-efficient ($\frac{4906.95}{4465.12} - 1 \approx 9.89\%$ lesser required GPU memory) and yields better results ($\frac{12.27}{9.71} - 1 \approx 26.36\%$ shorter training time and $\frac{5.780}{5.752} - 1 \approx 0.48\%$ shorter length) than the original RL strategy.

V. CONCLUSION

Our study proposes NAR4TSP, the first NAR model trained with RL for solving TSPs. Through extensive experimentation comparing NAR4TSP with SOTA models, we demonstrate that NAR4TSP outperforms existing approaches in terms of solution quality, inference latency, and generalization ability. Our findings strongly suggest that NAR4TSP is by far the most suitable method for solving TSPs in real-time decision-making scenarios. Moreover, we believe our approach will provide valuable insights towards solving other CO problems.

While NAR4TSP demonstrates superior inference speed attributed to its one-shot nature of NAR decoding, it does

not present a significant advantage over the SOTA AR model [16] in terms of solution quality. To achieve a better trade-off between inference latency and solution quality, we plan to develop a semi auto-regressive variant of NAR4TSP, which will generate multiple nodes at each decoding step by utilizing the neighboring nodes' information.

REFERENCES

- [1] M. R. Garey and D. S. Johnson, *Computers and Intractability: A Guide to the Theory of NP-Completeness*. W. H. Freeman & Co., 1990.
- [2] M. Christiansen, K. Fagerholt, and D. Ronen, "Ship routing and scheduling: Status and perspectives," *Transportation Science*, vol. 38, pp. 1–18, 2004.
- [3] M. Charikar, S. Khuller, D. M. Mount, and G. Narasimhan, "Algorithms for facility location problems with outliers," in *Proceedings of Annual ACM-SIAM Symposium on Discrete Algorithms*, 2001, p. 642–651.
- [4] C. Moon, J. Kim, and S. Hur, "Integrated process planning and scheduling with minimizing total tardiness in multi-plants supply chain," *Computers and Industrial Engineering*, vol. 43, pp. 331–349, 2002.
- [5] Y. Zhong, J. Lin, L. Wang, and H. Zhang, "Discrete comprehensive learning particle swarm optimization algorithm with metropolis acceptance criterion for traveling salesman problem," *Swarm and Evolutionary Computation*, vol. 42, pp. 77–88, 2018.
- [6] N. Onizawa, K. Katsuki, D. Shin, W. J. Gross, and T. Hanyu, "Fast-converging simulated annealing for ising models based on integral stochastic computing," *IEEE Transactions on Neural Networks and Learning Systems*, pp. 1–7, 2022.
- [7] Y. Bengio, A. Lodi, and A. Prouvost, "Machine learning for combinatorial optimization: a methodological tour d'horizon," *European Journal of Operational Research*, vol. 290, pp. 405–421, 2021.
- [8] Z. Zhang, Z. Wu, H. Zhang, and J. Wang, "Meta-learning-based deep reinforcement learning for multiobjective optimization problems," *IEEE Transactions on Neural Networks and Learning Systems*, pp. 1–14, 2022.
- [9] Y. Shao, J. C. Lin, G. Srivastava, D. Guo, H. Zhang, H. Yi, and A. Jolfaei, "Multi-objective neural evolutionary algorithm for combinatorial optimization problems," *IEEE Transactions on Neural Networks and Learning Systems*, vol. 34, pp. 2133–2143, 2023.
- [10] Z. Zhang, H. Liu, M. Zhou, and J. Wang, "Solving dynamic traveling salesman problems with deep reinforcement learning," *IEEE Transactions on Neural Networks and Learning Systems*, vol. 34, pp. 2119–2132, 2023.
- [11] H. Gao, X. Zhou, X. Xu, Y. Lan, and Y. Xiao, "AMARL: An attention-based multiagent reinforcement learning approach to the min-max multiple traveling salesmen problem," *IEEE Transactions on Neural Networks and Learning Systems*, pp. 1–15, 2023.
- [12] A. Nowak, D. Folqué, and J. Bruna, "Divide and conquer networks," in *Proceedings of International Conference on Learning Representations*, 2018.
- [13] C. K. Joshi, T. Laurent, and X. Bresson, "An efficient graph convolutional network technique for the travelling salesman problem," in *Proceedings of INFORMS Annual Meeting, Session on Boosting Combinatorial Optimization using Machine Learning*, 2019.
- [14] D. L. Applegate, R. E. Bixby, V. Chvátal, and W. J. Cook, *The Traveling Salesman Problem: A Computational Study*. Princeton University Press, 2007.
- [15] W. Kool, H. van Hoof, and M. Welling, "Attention, learn to solve routing problems!" in *Proceedings of International Conference on Learning Representations*, 2019.
- [16] X. Bresson and T. Laurent, "The transformer network for the traveling salesman problem," *arXiv preprint arXiv:2103.03012*, 2021.
- [17] M. Jung, J. Lee, and J. Kim, "A lightweight CNN-transformer model for learning traveling salesman problems," *arXiv preprint arXiv:2305.01883*, 2023.
- [18] S. J. Rennie, E. Marcheret, Y. Mroueh, J. Ross, and V. Goel, "Self-critical sequence training for image captioning," in *Proceedings of IEEE Conference on Computer Vision and Pattern Recognition*, 2017, pp. 7008–7024.
- [19] O. Vinyals, M. Fortunato, and N. Jaitly, "Pointer networks," in *Proceedings of Advances in Neural Information Processing Systems*, 2015, pp. 2692–2700.
- [20] I. Bello, H. Pham, Q. V. Le, M. Norouzi, and S. Bengio, "Neural combinatorial optimization with reinforcement learning," in *Proceedings of International Conference on Learning Representations Workshop*, 2017.
- [21] E. Khalil, H. Dai, Y. Zhang, B. Dilkina, and L. Song, "Learning combinatorial optimization algorithms over graphs," in *Proceedings of Advances in Neural Information Processing Systems*, 2017, pp. 6351–6361.
- [22] M. Deudon, P. Cournut, A. Lacoste, Y. Adulyasak, and L. M. Rousseau, "Learning heuristics for the TSP by policy gradient," in *Proceedings of Integration of Constraint Programming, Artificial Intelligence, and Operations Research*, 2018, pp. 170–181.
- [23] Y. Wu, W. Song, Z. Cao, J. Zhang, and A. Lim, "Learning improvement heuristics for solving routing problems," *IEEE Transactions on Neural Networks and Learning Systems*, vol. 33, pp. 5057–5069, 2022.
- [24] P. da Costa, J. Rhuggenaath, Y. Zhang, A. Akcay, and U. Kaymak, "Learning 2-opt heuristics for routing problems via deep reinforcement learning," *SN Computer Science*, vol. 2, pp. 1–16, 2021.
- [25] C. K. Joshi, Q. Cappart, L.-M. Rousseau, and T. Laurent, "Learning the travelling salesperson problem requires rethinking generalization," *Constraints*, vol. 27, pp. 70–98, 2022.
- [26] Q. Ma, S. Ge, D. He, D. Thaker, and I. Drori, "Combinatorial optimization by graph pointer networks and hierarchical reinforcement learning," in *Proceedings of AAAI Workshop on Deep Learning on Graphs: Methodologies and Applications*, 2020.
- [27] M. Nazari, A. Oroojlooy, M. Takáč, and L. V. Snyder, "Reinforcement learning for solving the vehicle routing problem," in *Proceedings of Advances in Neural Information Processing Systems*, 2018, pp. 9861–9871.
- [28] Q. Wang, K. H. Lai, and C. Tang, "Solving combinatorial optimization problems over graphs with bert-based deep reinforcement learning," *Information Sciences*, vol. 619, pp. 930–946, 2023.
- [29] M. Padberg and G. Rinaldi, "A branch-and-cut algorithm for the resolution of large-scale symmetric traveling salesman problems," *SIAM Review*, vol. 33, pp. 60–100, 1991.
- [30] D. Applegate, R. Bixby, V. Chvátal, and W. Cook, "Implementing the Dantzig-Fulkerson-Johnson algorithm for large traveling salesman problems," *Mathematical Programming*, vol. 97, pp. 91–153, 2003.
- [31] R. Bellman, "Dynamic programming treatment of the travelling salesman problem," *Journal of the ACM*, vol. 9, pp. 61–63, 1962.
- [32] D. S. Hochba, "Approximation algorithms for np-hard problems," *SIGACT News*, vol. 28, p. 40–52, 1997.
- [33] K. Helsgaun, "An extension of the Lin-Kernighan-Helsgaun TSP solver for constrained traveling salesman and vehicle routing problems," *Roskilde: Roskilde University*, pp. 24–50, 2017.
- [34] K. Helsgaun, "General k-opt submoves for the Lin-Kernighan TSP heuristic," *Mathematical Programming Computation*, pp. 119–163, 2009.
- [35] W. Kool, H. van Hoof, J. Gromicho, and M. Welling, "Deep policy dynamic programming for vehicle routing problems," in *Proceedings of International Conference on Integration of Constraint Programming, Artificial Intelligence, and Operations Research*, 2022, pp. 190–213.
- [36] W. Deng, L. Zhang, X. Zhou, Y. Zhou, Y. Sun, W. Zhu, H. Chen, W. Deng, H. Chen, and H. Zhao, "Multi-strategy particle swarm and ant colony hybrid optimization for airport taxiway planning problem," *Information Sciences*, vol. 612, pp. 576–593, 2022.
- [37] W. Yang, D. Wang, W. Pang, A.-H. Tan, and Y. Zhou, "Goods consumed during transit in split delivery vehicle routing problems: Modeling and solution," *IEEE Access*, vol. 8, pp. 110 336–110 350, 2020.
- [38] K. Li, T. Zhang, R. Wang, W. Qin, H. He, and H. Huang, "Research reviews of combinatorial optimization methods based on deep reinforcement learning," *Zidonghua Xuebao/Acta Automatica Sinica*, vol. 47, pp. 2521–2537, 2021.
- [39] D. Bahdanau, K. Cho, and Y. Bengio, "Neural machine translation by jointly learning to align and translate," in *Proceedings of International Conference on Learning Representations*, 2015.
- [40] Z. Fu, K. Qiu, and H. Zha, "Generalize a small pre-trained model to arbitrarily large TSP instances," in *Proceedings of the AAAI Conference on Artificial Intelligence*, 2021, pp. 7474–7482.
- [41] D. Silver, J. Schrittwieser, K. Simonyan, I. Antonoglou, A. Huang, A. Guez, T. Hubert, L. Baker, M. Lai, A. Bolton, Y. Chen, T. P. Lillicrap, F. Hui, L. Sifre, G. van den Driessche, T. Graepel, and D. Hassabis, "Mastering the game of go without human knowledge," *Nature*, vol. 550, pp. 354–359, 2017.
- [42] V. Mnih, K. Kavukcuoglu, D. Silver, A. A. Rusu, J. Veness, M. G. Bellemare, A. Graves, M. A. Riedmiller, A. Fidjeland, G. Ostrovski, S. Petersen, C. Beattie, A. Sadik, I. Antonoglou, H. King, D. Kumaran, D. Wierstra, S. Legg, and D. Hassabis, "Human-level control through deep reinforcement learning," *Nature*, vol. 518, pp. 529–533, 2015.
- [43] A. Vaswani, N. Shazeer, N. Parmar, J. Uszkoreit, L. Jones, A. N. Gomez, Ł. Kaiser, and I. Polosukhin, "Attention is all you need," in *Proceedings*

- of *Advances in Neural Information Processing Systems*, 2017, pp. 6000–6010.
- [44] Q. Ran, Y. Lin, P. Li, and J. Zhou, “Guiding non-autoregressive neural machine translation decoding with reordering information,” in *Proceedings of the AAAI Conference on Artificial Intelligence*, 2021, pp. 13 727–13 735.
 - [45] P. Koehn and R. Knowles, “Six challenges for neural machine translation,” in *Proceedings of Association for Computational Linguistics Workshop*, 2017, pp. 28–39.
 - [46] D. Liben-Nowell and J. Kleinberg, “The link prediction problem for social networks,” in *Proceedings of International Conference on Information and Knowledge Management*, 2003, pp. 556–559.
 - [47] L. Wang, Y. Xiao, J. Li, X. Feng, Q. Li, and J. Yang, “HIRWR: Internal inclined random walk with restart for lncRNA-disease association prediction,” *IEEE Access*, vol. 7, pp. 54 034–54 041, 2019.
 - [48] Y. Xiao, Z. Xiao, X. Feng, Z. Chen, L. Kuang, and L. Wang, “A novel computational model for predicting potential lncRNA-disease associations based on both direct and indirect features of lncRNA-disease pairs,” *BMC Bioinformatics*, vol. 21, pp. 1–22, 2020.
 - [49] F. Stahlberg, “Neural machine translation: A review,” *Journal of Artificial Intelligence Research*, vol. 69, pp. 343–418, 2020.
 - [50] B. Hudson, Q. Li, M. Malencia, and A. Prorok, “Graph neural network guided local search for the traveling salesperson problem,” in *Proceedings of International Conference on Learning Representations*, 2022.
 - [51] P. Veličković, G. Cucurull, A. Casanova, A. Romero, P. Liò, and Y. Bengio, “Graph attention networks,” in *Proceedings of International Conference on Learning Representations*, 2018.
 - [52] S. Ioffe and C. Szegedy, “Batch normalization: Accelerating deep network training by reducing internal covariate shift,” in *Proceedings of International Conference on Machine Learning*, 2015, pp. 448–456.
 - [53] Z. Wang, J. Chen, and H. Chen, “EGAT: Edge-featured graph attention network,” in *Proceedings of Artificial Neural Networks and Machine Learning*, 2021, pp. 253–264.
 - [54] R. J. Williams, “Simple statistical gradient-following algorithms for connectionist reinforcement learning,” *Machine Learning*, vol. 8, pp. 229–256, 1992.
 - [55] D. P. Kingma and J. Ba, “Adam: A method for stochastic optimization,” in *Proceedings of International Conference on Learning Representations*, 2014.
 - [56] Y.-D. Kwon, J. Choo, B. Kim, I. Yoon, Y. Gwon, and S. Min, “POMO: Policy optimization with multiple optima for reinforcement learning,” in *Proceedings of Advances in Neural Information Processing Systems*, 2020, pp. 21 188–21 198.